Int. J. Electrochem. Sci., 15 **(2020)** 8479 – 8497, doi: 10.20964/2020.09.80

International Journal of
ELECTROCHEMICAL
SCIENCE
www.electrochemsci.org

Study on Growth of Corrosion Scale on Various Iron Based Materials (Grey cast iron/Carbon steel/Ductile Iron) in Water Distribution Systems

Hao Guo[1,*], *Haolin Chen*[2], *Haiya Zhang*[3], *Xingfei Liu*[2], *Ying Chen*[2], *Yimei Tian*[2], *Jianhua Yin*[4]

[1] The Institute of Seawater Desalination and Multipurpose Utilization, MNR(Tianjin), Tianjin 300192, China
[2] School of Environmental Science and Engineering，Tianjin University, Tianjin 300350, China
[3] School of Environment, Tsinghua University, Beijing, 100084, China
[4] Tianjin Zhonghai Water Treatment Technology Co., Ltd., Tianjin 300192, China
[*]E-mail: tjguohao@163.com

Received: 3 May 2020 / *Accepted:* 13 July 2020 / *Published:* 10 August 2020

A six-month corrosion experiment was conducted to examine the corrosion behaviour and scale growth of common iron materials (grey cast iron, carbon steel and ductile iron) in a simulated flow corrosion system. Coupon tests, electrochemical measurements and microanalysis were integrated to reveal the intrinsic connection between corrosion rate variation and physicochemical characteristics of corrosion scales, i.e., the corrosion control mechanism of the scales. The coupon tests showed ductile iron has the lowest corrosion rate and most stable corrosion scales. The EIS analysis confirmed that the corrosion scales have an effective control function for the electrochemical corrosion process. The outer scale layer of grey cast iron and carbon steel was more protective than the inner layer. However, for ductile iron, both the outer and inner layers of the scales were sufficiently dense to inhibit the corrosion process. The scale physicochemical analysis demonstrated the diversity of corrosion product composition and further confirmed the protect mechanism of the pipe scales: an effective corrosion-control scale layer is formed with a high content of stable α-FeOOH and $CaCO_3$ deposition, which limits the mass diffusion of the electrochemical corrosion process.

Keywords: Corrosion scales; Coupon test; EIS; Iron pipe; Water distribution system

1. INTRODUCTION

Iron pipes are widely used in water distribution systems (WDS) in China[1], and their corrosion is the main cause of pipe leakage and burst. With long-term service, irregular corrosion scales generated on the inner wall of the pipe reduce the conveying capacity of the WDS and cause the "red

water" phenomenon due to iron release[2]. Therefore, the corrosion behaviour and scale characteristics of iron pipes are of great significance for the stability of water quality and control of WDS corrosion.

The corrosion behaviour of WDS pipes is usually studied by corrosion simulation experiments, using metal coupons for weight-loss tests or using a metal working electrode for electrochemical measurements. Among these methods, the weight-loss method is mainly used to study the variation of the corrosion rate in different hydraulic and water quality conditions. Based on its advantages of real-time and in situ monitoring of the corrosion process, the electrochemical test can be employed to investigate the electrochemical corrosion mechanism. Liu et al.[3] studied the variation of the corrosion rate of a ductile pipe in drinking water using the weight-loss method. The results showed that in tap water, the corrosion rate of ductile iron greatly fluctuated in the early stage, gradually declined with time, and finally stabilized at approximately 48 hours. Masters et al.[4] established a simulated WDS to study the effect of disinfectant types on pipe corrosion. The results showed that the corrosion rate caused by free chlorine was approximately four times that caused by chloramine. Wang[5] studied the effects of five corrosion influencing factors on the inner corrosion of grey cast iron using coupon tests. The results showed that the order of importance of the influencing factors obtained by the grey correlation analysis was as follows: residual chlorine > sodium chloride > dissolved oxygen > temperature > pH. Sancy et al.[6] adopted the EIS measurement to investigate the corrosion product characteristics in tap water and found that the porous corrosion product layer on the electrode surface hindered the diffusion of cathodic depolarization agent and had a certain inhibitory effect on corrosion. Rios et al.[7] employed the rotating cylinder electrode (RCE) to study the electrochemical corrosion behaviour of copper, carbon steel and 304 stainless steel in tap water, and the results showed that the corrosion resistances of different metals were mainly related to the state of the surface corrosion product film. Fabbricino et al.[8] studied the variation of corrosion potential (E_{corr}) of iron in stagnant and flowing tap water, and their results showed that the on-site measurement of E_{corr} was a practical and rapid method to determine the effects of changes in hydraulic conditions and water quality on pipe corrosion.

Recently, researchers have attempted to combine electrochemical measurement with the weight-loss method to conduct corrosion studies. Zou et al.[9] used the polarization curve test and weight-loss method to measure the corrosion rate of mild steel that was immersed in seawater for a long duration, and they found that the polarization curve produced a certain error due to the high electrochemical activity of the rust layer. Finally, an accurate calibration method was presented. In addition, the author's research group integrated the electrochemical method with the coupon test and conducted several experiments under flowing drinking water[10-11] to reveal the growth mechanism of corrosion scales and the effect of the mechanism on the corrosion process of ductile iron, and the physical model of scale growth was established.

Corrosion scales were usually taken from old pipes for physical and chemical analyses, including element composition and crystal structure determination. Świetlik et al.[12] used the XRD method to examine the wet scale sample and found that the scale contained a large amount of unstable state green rusts (GRs). GRs transform into the more stable α-FeOOH and γ-FeOOH in the drying process of the samples. This study provides a new method of scale composition analysis. Yang et al.[13] found that magnetite (M) and goethite (G) were the main components of pipe scales in different

water supply histories, but the mass ratio of magnetite to goethite (M/G) varied significantly due to the effect of the scale structure and water source conditions. The M/G ratio can be used to evaluate the performance of pipe scales under different water source conditions. In addition, researchers studied the effects of water quality, biofilms and disinfectants on corrosion scales. Li et al.[14] investigated the effects of chlorine and chloramine disinfection on pipe scales of cast iron and found that the scales formed under chlorine disinfection were relatively loose, while a dense corrosion scale could easily be formed by chloramine disinfection. Li et al.[15] compared the scale characteristics of pipes transporting groundwater and surface water. The results showed that nitrate-reducing bacteria associated with iron cycle in the biofilm played an important role in the formation of Fe_3O_4 in pipe scales. Wang et al.[16] used an annular reactor to study the effect of O_3/Cl_2 disinfection on pipe scales, and the results showed that after the O_3/Cl_2 disinfection treatment, a higher content of iron-oxidizing bacteria and iron-reducing bacteria in the pipe scale biofilm corresponded to a higher content of Fe_3O_4 in the pipe scales. The pipe scales were more stable than that generated in the Cl_2-only disinfection treatment.

In recent years, researchers have paid special attention to the effect of the dissolution of corrosion scales on the water quality, particularly the release of metal pollutants caused by pipe scales. Hu et al.[17] studied the effect of the water quality change on the iron release of cast iron in mixed water (mixed surface water and underground water). Their results showed that Cl^- and SO_4^{2-} promoted the release of iron, while calcium hardness and alkalinity had the opposite trend; changing the disinfectant from free chlorine into chloramine could mildly inhibit the iron release, and the dissolved oxygen consumption was significantly associated with iron release. Furthermore, release behaviour research on other pollutants concentrated in pipe scales has emerged with the increasingly stringent requirements on water quality safety. Trueman and Gagnon[18] studied the relationship between lead release and iron release from corroded water pipes and found that when a short circuit of lead and Fe_3O_4 formed, the lead release rate significantly increased. They inferred that the lead dissolved into drinking water with colloidal particles of the iron scales. Sun et al.[19] studied the effects of sulfate on the release process of trace heavy metals in the pipe scales in different water environments (groundwater and surface water). The results showed that an increase in sulfate content could cause the release of manganese, nickel, copper, lead, chromium, arsenic and other heavy metals, but the quantity released was gradually reduced with increasing time. By continuously monitoring the metal pollutant release in the actual WDS, Li et al.[20] concluded that Mn and Al were more easily released back to water than iron during the process of flushing the pipes, and there was an obvious co-release behaviour of particle-state Mn and Al.

Although great progress has been made in the research on the corrosion behaviour and corrosion scales, there is no perfect combination of the two studies. Corrosion research by electrochemical test can provide more abundant information on the corrosion mechanism, but because the working surfaces are often less than 1 cm^2, it is difficult to simulate the actual pipe scale growth progress. Meanwhile, corrosion scale physicochemical property studies through the old pipe sections cannot obtain dynamic information on scale growth and development, which is of great importance to corrosion control and forecast of pipes in WDS. Therefore, a specific electrochemical test device, where corrosion test coupons can be directly used as the working electrode, was designed in this study.

With a larger surface area than the common electrode, the test coupon under a simulated flow corrosion device can better simulate the corrosion process of the inner wall of a WDS pipe, and the corrosion products generated on the coupon surface are much more similar to actual pipe scales. Then, the corroded coupon is directly fixed to the electrochemical test device as the working electrode for electrochemical measurement. Thus, the corrosion rate variation, scale morphology and physicochemical properties, and electrochemical corrosion reaction information can be acquired at the same time, which can more precisely reveal the intrinsic connection between the corrosion rate variation and physicochemical characteristics of corrosion scales in WDS.

2. EXPERIMENTAL

2.1 Experiment device

Figure 1 shows the schematic of the simulated flow corrosion system (SFCS). This system includes: (I) a drinking water storage tank, (II) a piping system, and (III) internal corrosion test units. The storage tank is a 500-litre polyethylene bucket filled with tap water. Water is pumped from the tank into the piping system, where the outfall simultaneously discharges and circulates the water. Thus, the SFCS can provide a corrosion environment similar to that of the actual WDS. The internal corrosion test unit is a PMMA (polymethyl methacrylate) cuboid container (3 cm×10 cm×18 cm). Each unit comprises six test coupons, and the coupon surface is parallel to the direction of water flow to simulate the internal corrosion of the pipeline. One of six coupons is used for the electrochemical measurement, and the other five pieces are used for the corrosion rate monitoring and corrosion product analysis. In this study, eighteen test units were set up for three types of iron materials: cast iron, carbon steel and ductile iron.

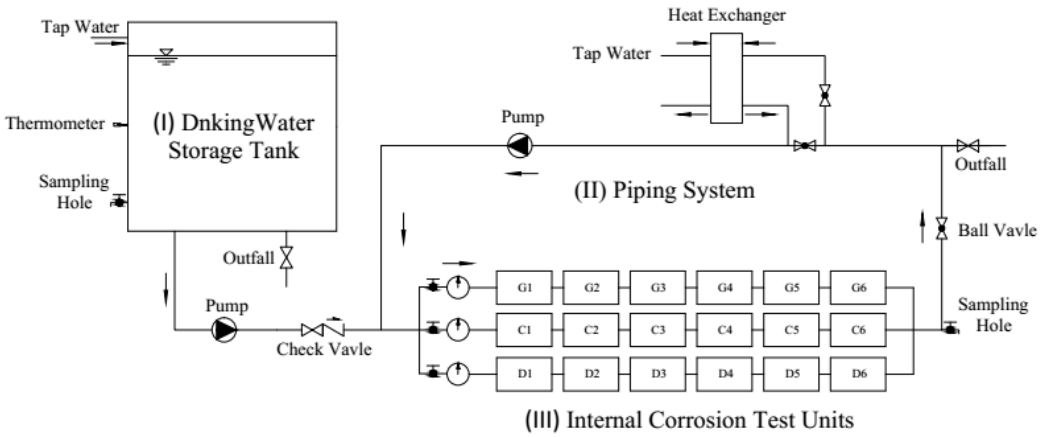

Figure 1. Schematic of the simulated flow corrosion system

Figure 2 shows the schematic of the electrochemical measurement cell (EMC). The cell consists of an annealed glass cylinder and a PTFE (polytetrafluoroethylene) plug. In the EMC, the test coupon can be directly fixed at point A as a working electrode by fixing bolt D. The reference

electrode (B) - saturated calomel electrode (SCE) is inserted into the glass salt bridge, which is filled with saturated potassium NaCl(aq). At the other end of the cell, a large swatch of platinum mesh serves as the counter electrode (C).

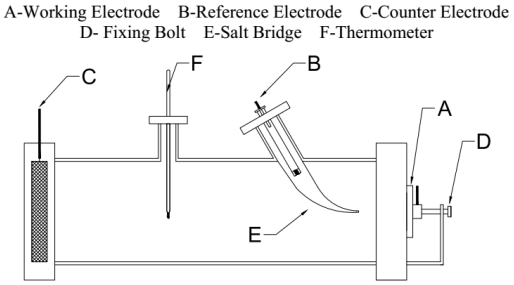

Figure 2. Schematic of the electrochemical measurement cell

2.2 Test coupon and tap water

Type-I standard test coupons (25 mm×5 mm×2 mm) were used in this experiment. The test coupons were first polished by sandpaper and subsequently rinsed with distilled water, a pickling solution, an alkaline solution, and ethanol. Then, they were dried in a desiccator for 24 hours on standby. To distinguish the three materials, G, C and D denote grey cast iron, carbon steel and ductile iron, respectively. The composition of the test coupon (provided by the manufacturer) is shown in Table 1.

Table 1. Composition of three types of test coupons（wt%）

Materials	C	Si	Mn	P	S	Mg	Re	Fe
G	3.48	2.32	0.55	0.09	0.10	—	—	93.46
C	0.20	0.30	0.68	0.04	0.05	—	—	98.73
D	3.60	2.60	0.45	0.06	0.02	0.04	0.03	93.20

The tap water in the experiment comes from the WDS of Tianjin, China, and is taken directly from the faucet of the laboratory. Water quality indicators were monitored every two weeks during the test, and the average values of each indicator are shown in Table 2.

Table 2. Water quality parameters of tap water

Parameter	Water quality[a]
pH	7.13±0.30
DO ($mg \cdot L^{-1}$)	6.27±0.38
Total hardness ($mg \cdot L^{-1}$ as $CaCO_3$)	237.16±9.5
Total alkalinity ($mg \cdot L^{-1}$ as $CaCO_3$)	112.11±6.5
Cl^- ($mg \cdot L^{-1}$)	48.96±1.6

SO_4^{2-} ($mg \cdot L^{-1}$)	105.85±7.6
Total residual chlorine ($mg \cdot L^{-1}$)	0.23±0.04
Conductivity ($\mu s \cdot cm^{-1}$)	550±7.6
TDS ($mg \cdot L^{-1}$)	190±4.2

[a]Mean±standard deviation

2.3 Experiment method

A long-term flow corrosion test of six months was performed with the SFCS. The test units were sampled on days 30, 60, 90, 120, 150 and 180. The corroded coupons were first photographed with a high-definition digital camera to obtain the corrosion morphologies. Then, a representative piece of coupon was selected for the electrochemical corrosion measurement. Corrosion products of the remaining coupons were used for the microscopic analysis, and the bare coupons were weighed to obtain the corrosion rate.

2.3.1 Corrosion rate measurement

Before the experiment, the dry test coupon should be weighed by an analytical balance (with an accuracy of 10^{-4} g) to obtain the initial mass. After the corrosion test, the coupons removed from the SFCS were cleaned and dried according the aforementioned standard procedure. Then, the final mass was weighed and recorded.

2.3.2 Electrochemical measurement

A typical corroded coupon removed from the SFCS was installed into the EMC, and an EIS measurement was conducted to obtain the electrochemical characteristics of the corrosion scale. Before each EIS measurement, the steady-state open circuit potential (OCP) was recorded. Then, EIS was performed on the steady-state OCP, which was driven at an applied-amplitude alternating current (AC) signal of 10 mV and a frequency range from 100 kHz to 10 mHz. Zview 2.0 was used to collect the EIS data, and ZsimpWin 3.10 was used to fit the parameters.

2.3.3 Scale physicochemical characteristic analysis

The corrosion products removed from the corroded coupons are stored in the dryer to avoid air oxidation. The entire scale layer was sprayed with gold to prepare the sample, and then SEM (Nanosem 430) observation and EDS analysis were conducted. The scale sample was ground into powder for the XRD (D/max-2500) analysis, where 2θ was 10-90°.

3. RESULTS AND DISCUSSION

3.1 Scale morphology observation

Figure 3 shows the typical photographs of the test coupons to show the growth of the corrosion scales of grey cast iron (G), carbon steel (C) and ductile iron (D) in the six-month simulated corrosion test. With increasing time of the experiment, the corrosion scales produced on the three types of coupons grew from thin to thick, from smooth to rough, and from uniform to uneven. During the experiment, due to the flushing effect of the water flow, parts of the scales randomly fell off, which resulted in inhomogeneous scales. By comparing the scale morphologies of the three materials after 6 months of corrosion, we find that the scales of grey cast iron and carbon steel are relatively thicker, looser and rougher, and there are traces of water flow on the scale surface. In contrast, the corrosion scale of ductile iron is relatively thinner and denser, although its surface is also uneven and rough.

On the whole, uniform corrosion is predominant in the initial corrosion period, such that the corrosion products cover the entire coupon surface. However, due to the looseness and low adhesion of scales, flowing water can easily wash parts of the scales away and generate defects on the scale surface. Thus, after three months of water flushing, the dominant form of corrosion becomes localized corrosion, and the trend will be increasingly obvious with the increase in corrosion time. Compared with the corrosion scales taken from old pipes used for decades [21, 22], the new-generated (less than 6 months) corrosion scales presented no obvious layers and there was no shell-like layer covering the surface of the scales. Thus, the growth of the scales was a very long process and the morphologies of scales were determined by the material and corrosion environment (including water quality and hydraulic condition).

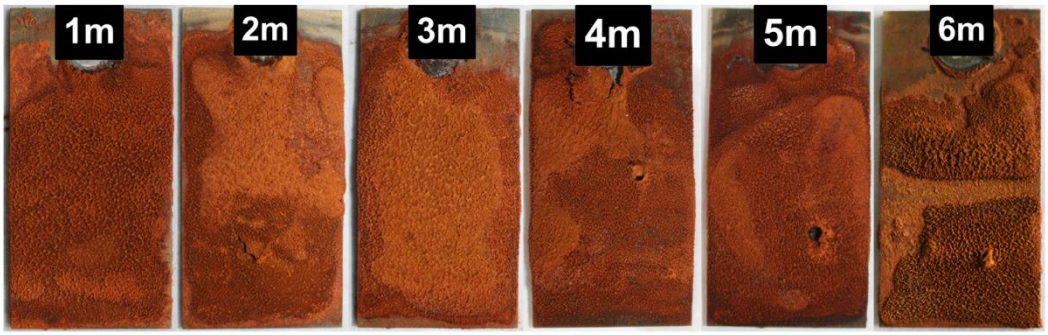

(a) Grey cast iron

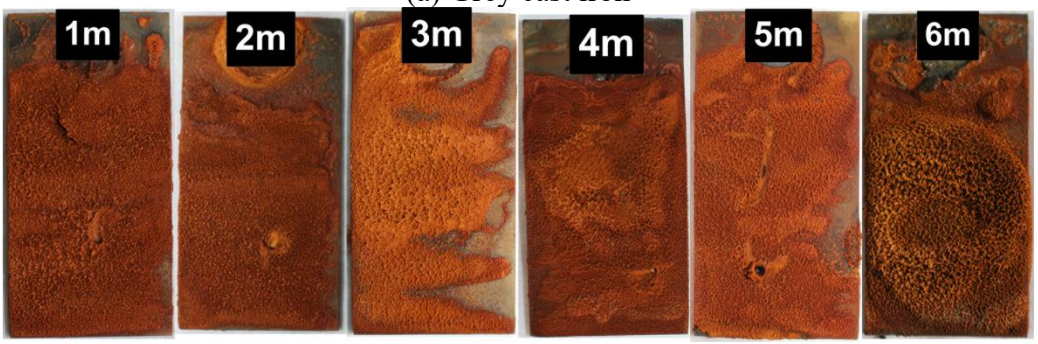

(b) Carbon steel

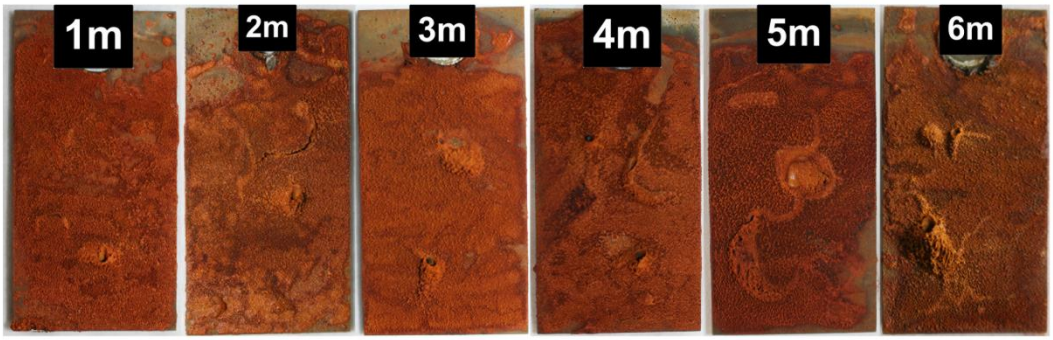

(c) Ductile iron

Figure 3. Morphologies of corrosion scales at different corrosion times in SFCS. Corroded coupons were sampled on days 30, 60, 90, 120, 150 and 180. Experimental conditions: pH = 7.13±0.30, DO ($mg \cdot L^{-1}$) = 6.27±0.38, Total hardness ($mg \cdot L^{-1}$ as CaCO3) = 237.16±9.5, Total alkalinity ($mg \cdot L^{-1}$ as CaCO3) = 112.11±6.5, Cl^- ($mg \cdot L^{-1}$) = 48.96±1.6, SO42- ($mg \cdot L^{-1}$) = 105.85±7.6, Total residual chlorine ($mg \cdot L^{-1}$) = 0.23±0.04.

3.2 Corrosion rate variation

The corrosion rate can be calculated by the mass loss of test coupons, which were regularly removed from the SFCS. In this paper, the average corrosion rate (v_{aver}) of two sampling points is calculated by the mass loss of the two test coupons. Thus, the change in corrosion rate with time can be better reflected. The calculation formula of v_{aver} is shown in Equation 1.

$$v_{aver} = 87600 \times \frac{m_{(i-1)} - m_i}{S\rho t_i} \quad (1)$$

where v_{aver} is the average corrosion rate, $mm \cdot a^{-1}$; m_i and $m_{(i-1)}$ are the coupon weights of samplings i and (i-1), respectively, g; S is the exposed surface area, cm^2; ρ is the coupon density, g/cm^3; t_i is the interval corrosion time between samplings i and (i-1), h.

Figure 4 shows the variations of the average corrosion rate of three materials with increasing corrosion time. The corrosion rates of the three materials gradually decrease on the whole. Grey cast iron had the highest corrosion rates (from 0.2022 $mm \cdot a^{-1}$ to 0.0950 $mm \cdot a^{-1}$), carbon steel had the medium corrosion rates (from 0.0940 $mm \cdot a^{-1}$ to 0.0652 $mm \cdot a^{-1}$), and ductile iron had the lowest corrosion rates (from 0.0873 $mm \cdot a^{-1}$ to 0.0544 $mm \cdot a^{-1}$). The corrosion rate of grey cast iron shows a more obvious downward trend than those of carbon steel and ductile iron in the 6-month flow corrosion experiment: a sharp decline in the early period (months 1-3) and a moderate decline in the later period (months 4-6). Considering that the three materials are in almost identical corrosion environments, the corrosion products of grey cast iron have poorer inhibition effect on the corrosion process than the other two. The overall corrosion rates of carbon steel and ductile iron are relatively low, and the fluctuation is gentle, which indicates that the corrosion products have a good corrosion inhibition effect, good compactness, good adhesion, and good resistance to the flushing of water flow. Overall, ductile iron has the lowest corrosion rate, smallest fluctuation and most stable corrosion scales. And the order of corrosion rate is G > C > D, which further supports the necessity of replacing the cast iron pipe and steel pipe with the ductile iron pipe in WDS.

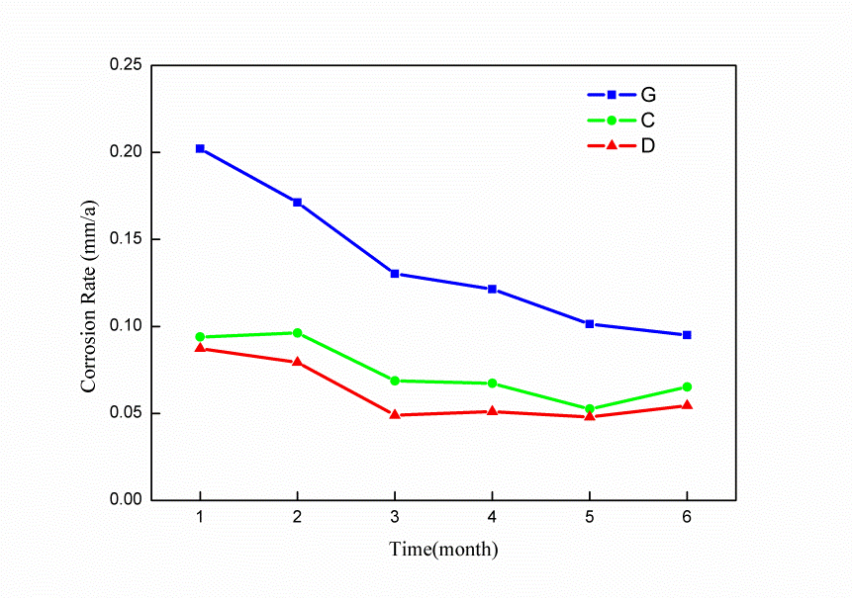

Figure 4. Variation of the average corrosion rate with increasing corrosion time. Corroded coupons were sampled and weighted on days 30, 60, 90, 120, 150 and 180. G, C and D denote grey cast iron, carbon steel and ductile iron, respectively.

3.3 Electrochemical measurement analysis

3.3.1 OCP variation

Since the OCP changes with the growth of corrosion scales, it can reflect the corrosion tendency of iron pipes. Figure 5 shows the variation of steady-state OCP recorded before each EIS measurement.

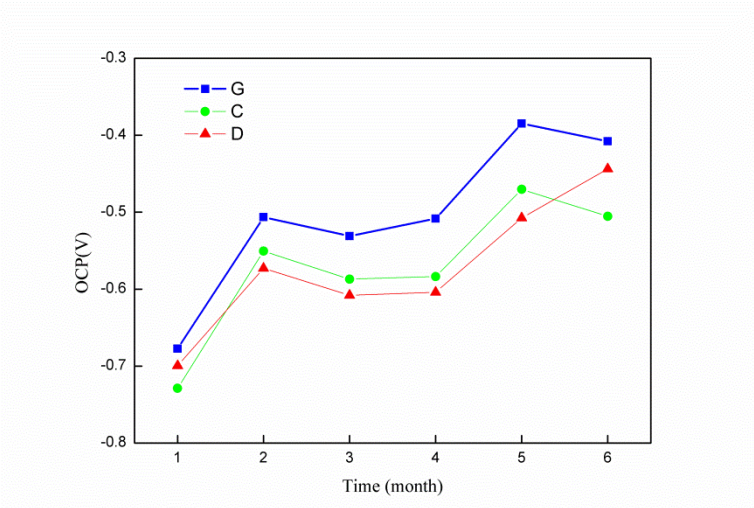

Figure 5. Variation of the OCP with increasing corrosion time. Corroded coupons removed from the SFCS were installed into the EMC for OCP measurement on days 30, 60, 90, 120, 150 and 180. G, C and D denote grey cast iron, carbon steel and ductile iron, respectively.

With the increase in flow corrosion time, the OCP of the three materials obviously increased

with fluctuation, which indicates that the corrosion tendency was weakened by the formation of the corrosion scales. Meanwhile, in the flow corrosion environment, the stability of the corrosion scales was easily affected by the environment. Although grey cast iron had a higher OCP than carbon steel and ductile iron, it also had a higher corrosion rate than both, which indicates that there is no corresponding consistent relationship between OCP and corrosion rate. Therefore, the actual corrosion rate of pipes cannot be determined by comparing OCP in practice.

3.3.2 EIS analysis

By conducting electrochemical tests on the test coupons covered with scales, the effect of the corrosion scale structure on metal corrosion can be investigated. Figure 6 shows the impedance plots of three types of materials measured in different corrosion times. With the growth of the corrosion scales, three types of Nyquist plots appeared. The Type-I plot consists of a high-frequency tail and two capacitive loops (a middle-frequency capacitive loop and a low-frequency capacitive loop), Type II consists of two capacitive loops (high-frequency and low-frequency) and Warburg diffusion impedance, and Type III consists of three capacitive loops (high-frequency, middle-frequency and low-frequency) and Warburg diffusion impedance.

The high-frequency tail or capacitive loop is typically related to the surface film of insoluble corrosion products[23,24], which corresponds to the outer layer of the corrosion scale. The middle- and low-frequency capacitive loops are associated with the inner layer of the corrosion scales and the electrical double layer, respectively. The appearance of Warburg diffusion impedance indicates that the corrosion scales are sufficiently dense, and the diffusion control of the corrosion process occurs. According to the references[25] and previous research results of the author[10], this paper intends to adopt the following three equivalent circuits to fit the EIS data. Due to the inhomogeneities of the corrosion scales, a constant-phase element (CPE) capacitor is used to represent the capacitance of the scales in the equivalent circuit. The pseudocapacitance associated with the CPE (C, $F \cdot cm^{-2}$) was calculated using Equation 2[26]:

$$C = \frac{(Y_o R)^{1/n}}{R} \qquad (2)$$

where parameter Y_o is in $S \cdot sec^n \cdot cm^{-2}$, R is the electrical resistance in parallel with the CPE in $ohm \cdot cm^2$, and n is the CPE power.

The corresponding physical structure of the equivalent circuit is shown in Table 3. R_s is the solution resistance; Q_{cs}, Q_o and Q_i are the constant phase elements related to the corrosion scales, outer layer and inner layer, respectively; R_{cs}, R_o and R_i are the resistances of the corrosion scales, outer layer and inner layer, respectively; C_{dl} is the double-layer capacitance; R_{ct} is the charge-transfer resistance; and W_1 is the Warburg impedance.

As shown in Table 3, grey cast iron mainly formed a single-layer scale with Warburg impedance (G-2m, G-3m, G-5m, G-6m) and sometimes a double-layer scale without Warburg impedance (G-1m, G-4m), which indicates that the scales of grey cast iron is unstable and usually generates a weakly protective single-layer scale. Cast iron mainly formed a double-layer scale without Warburg impedance (C-1m, C-3m, C-4m, C-5m, C-6m) and a single-layer scale with Warburg

impedance only in the second month (C-2m), which indicates that the scales of cast iron form an unprotected double-layer. In contrast, the change in scale structure of ductile iron was very complex: it constantly switched among a double-layer scale without Warburg impedance (D-1m, D-3m, D-5m), a double-layer scale with Warburg impedance (D-2m, D-4m) and a single-layer scale with Warburg impedance (D-6m). Thus, ductile iron usually generated double-layer scales, and alternated between unprotected and protected double-layer scales, and finally transformed into a protective single layer. This is not consistent to our previous findings [10, 11]: after 16 days of immersion, ductile iron generated double-layer scales with finite layer diffusion impedance. The main reason for the transition from finite layer diffusion impedance to Warburg impedance is that the compactness increases with the growth of scales and the diffusion capacity of oxygen through the scales becomes weaker and weaker, resulting in mass diffusion turns to be the corrosion rate control step.

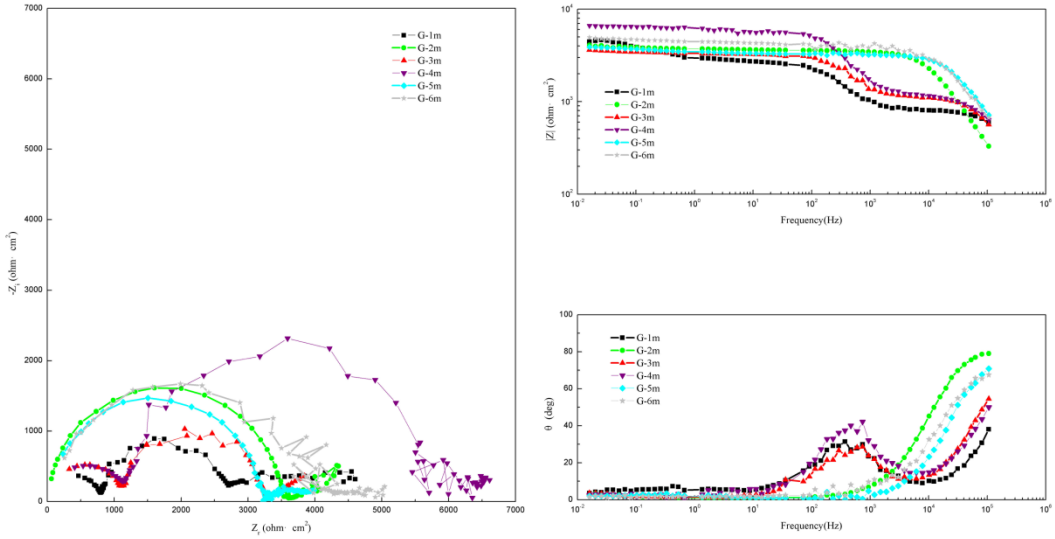

(a) Grey cast iron

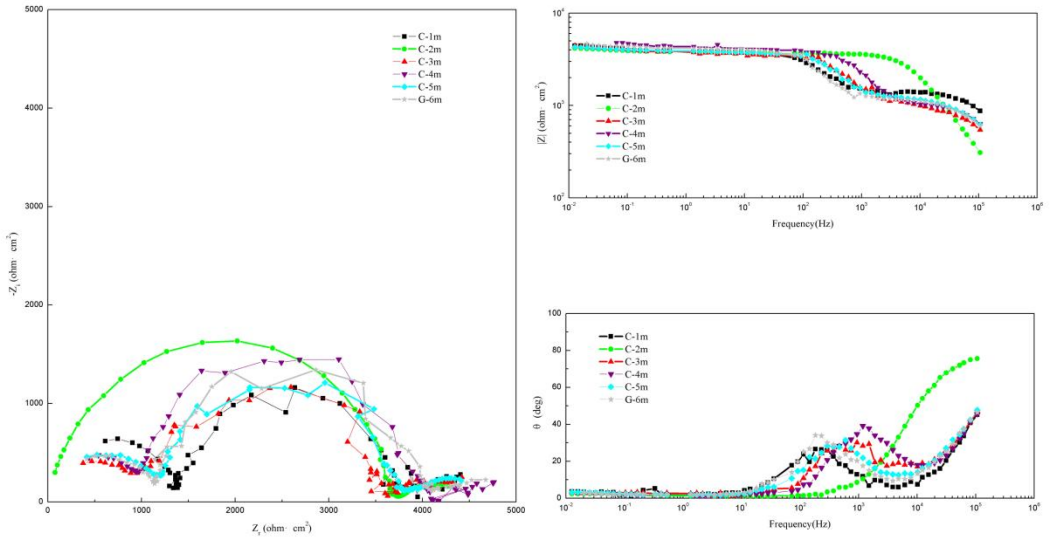

(b) Carbon steel

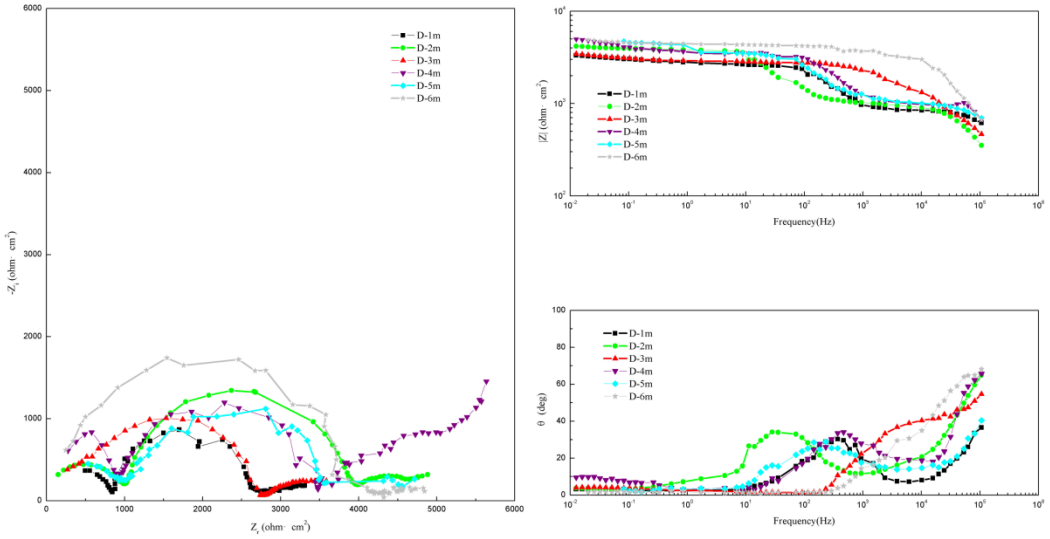

(c) Ductile iron

Figure 6. EIS plots measured at different corrosion time of the 1st, 2nd, 3rd, 4th, 5th, 6th month in EMC. Electrochemical measurement conditions: EIS testing range is from 100 kHz to 10 mHz with an amplitude of 10 mV.

Table 3. Physical models and equivalent circuits to fit the EIS plots

Type	Physical models and equivalent circuits	Corresponding EIS plots
I	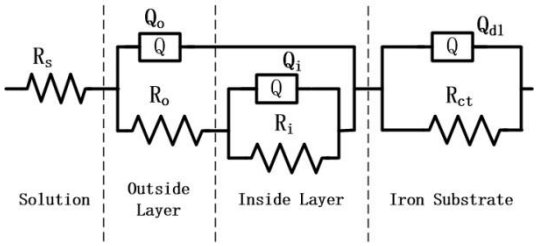	G-1m, G-4m; C-1m, C-3m, C-4m, C-5m, C-6m; D-1m, D-3m, D-5m;
II	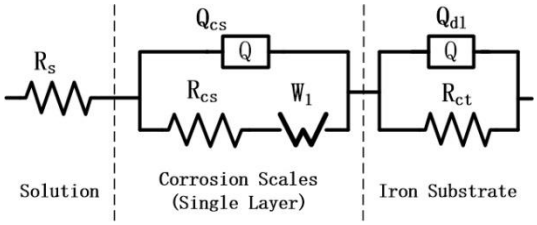	G-2m, G-3m, G-5m, G-6m; C-2m; D-6m;
III	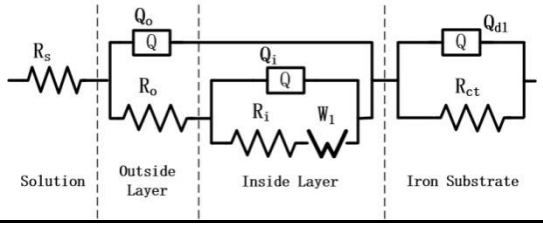	D-2m, D-4m;

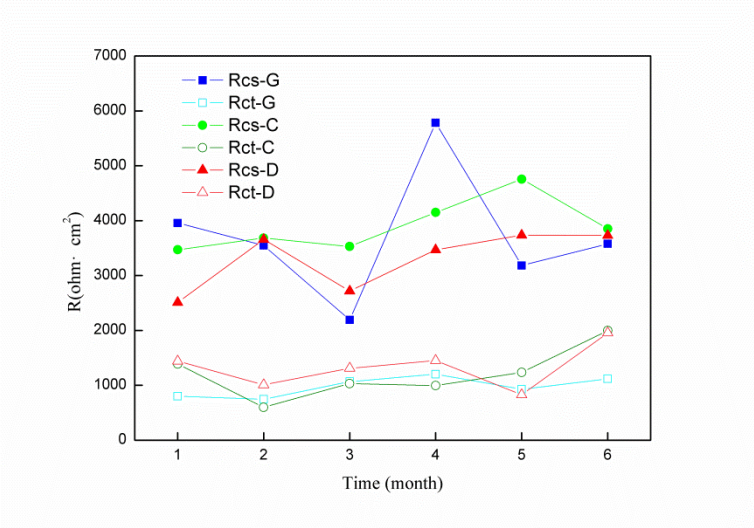

(a) R_{cs} and R_{ct}

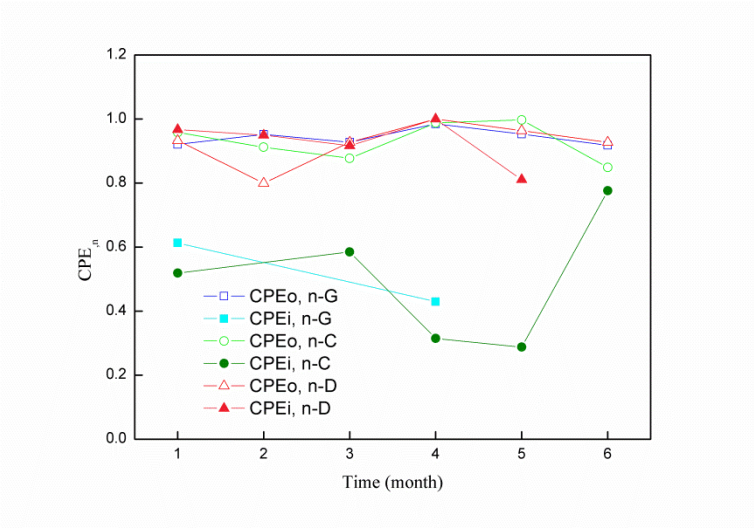

(b) CPE, n

Figure 7. Variation of EIS parameters obtained by fitting with the electrical circuits in Table 3. R_{cs} and R_{ct} are the resistance of corrosion scales and the charge-transfer resistance of corrosion scales; $CPE_{o,n}$ and $CPE_{i,n}$ are the CPE power of the outer and inner scale layer; G, C and D denote grey cast iron, carbon steel and ductile iron, respectively.

As shown in Table 3, three types of equivalent circuit were used to fit the corresponding EIS plots in different corrosion periods. The resistance of corrosion scales (R_{cs}) is a representative parameter to measure the growth of scales, and the power of CPE (CPE,n) in parallel with the scale resistance is related to the roughness and porosity of the scales[7]. When the corrosion scales form a double layer, the scale resistance is the sum of R_o and R_i. The fitting results are shown in Figure 7.

Figure 7(a) shows that the resistance of corrosion scales fluctuates between 2100~5800 ohm·cm^2, while the charge transfer resistance is stable at approximately 1000 ohm·cm^2, except for R_{ct}-C and R_{ct}-D (still under 2000 ohm·cm^2) during the 6th month. It can be seen that the equivalent resistance of corrosion scales of different materials was significantly higher than that of charge transfer resistance, which confirmed the controlling effect of corrosion scales on the electrochemical reaction.

From Figure 7(b), it can be found that, for grey cast iron and carbon steel, the CPE power of outer layer ($CPE_{o,n}$, >0.8) is always higher than the inner layer ($CPE_{i,n}$, <0.7), which indicates that the outer layer is more compact than the inner layer and the outer layer is more protective against pipe corrosion. This is consistent with previous research results [21, 22, 27]: most corrosion scales of cast iron pipe and galvanized steel pipe have a shell-like layer and a porous core. For the ductile iron, the COE,n of both the inner and outer layer is approximately 0.9, meaning that both the outer and inner scale layers are dense enough to inhibit the corrosion process. Therefore, it can be speculated that the effective inner scale layer of ductile iron is the key reason why the corrosion rate of ductile iron is lower than those of grey cast iron and carbon steel. The mechanism of corrosion inhibition of the scales is further revealed by the following study of the physical and chemical properties of scales.

3.4 Scales physicochemical characteristics

Figure 8 shows the SEM images of the corrosion scales after different corrosion times. Here, three groups (the 1st, 3rd, 6th month) of samples of each material are selected for display. The chemical compositions of the scales were characterized using EDS (Table 4), and the crystalline phase of the scales was determined by XRD (Figure 9).

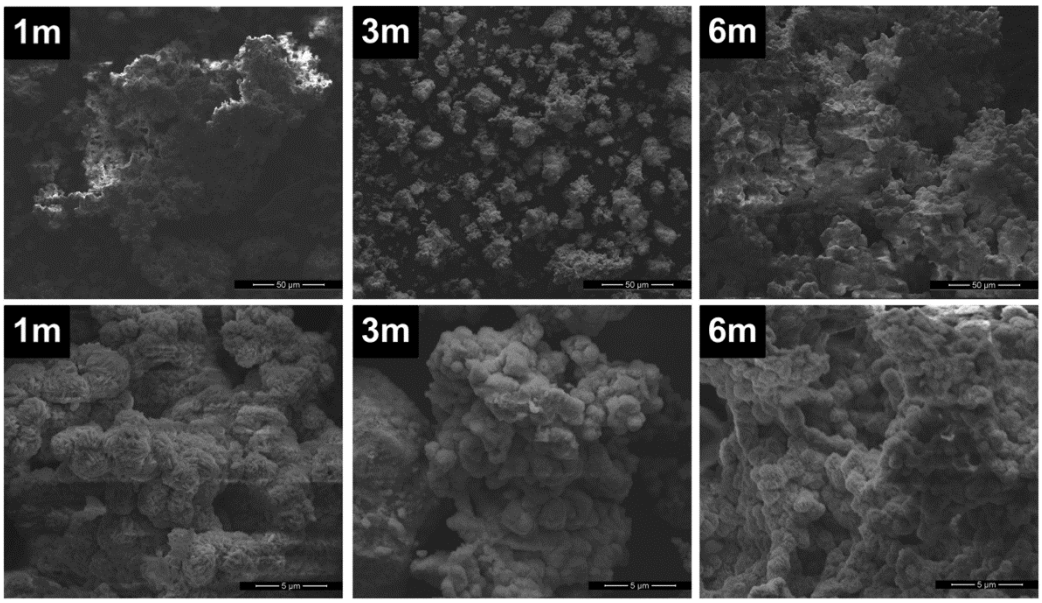

(a) Grey cast iron

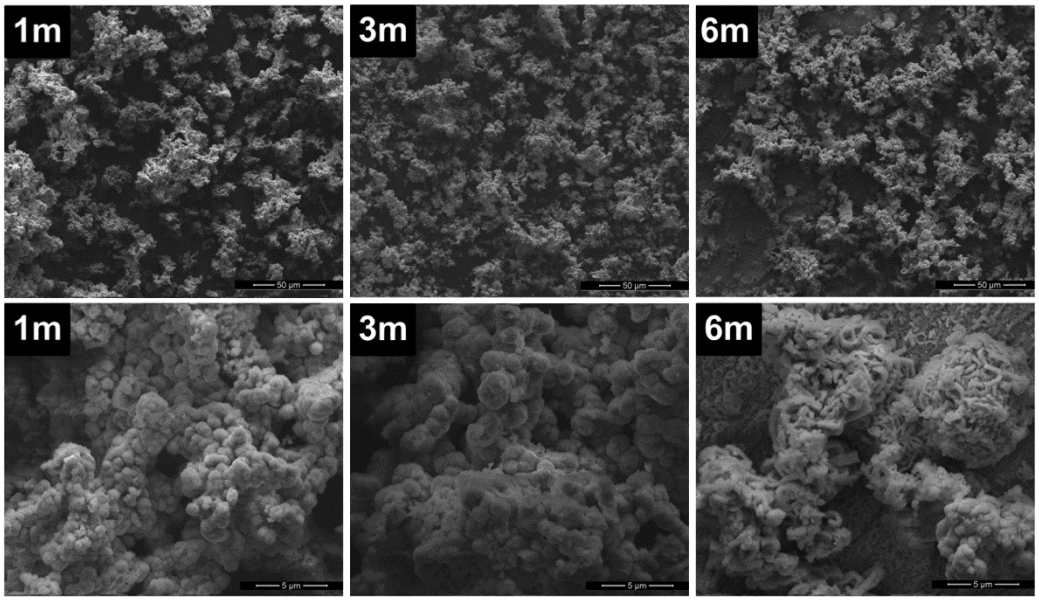

(b) Carbon steel

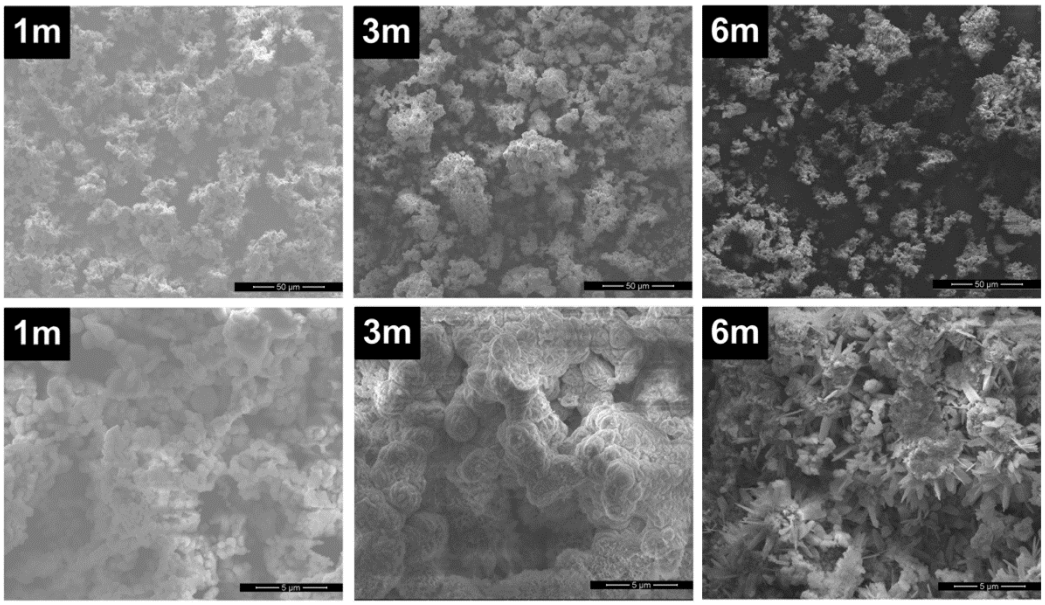

(c) Ductile iron

Figure 8. SEM images of the corrosion scales at different corrosion time of the 1st, 3rd and 6th month.

As seen from Figure 8, all the scales of 1st month were mainly amorphous and showed obvious porosity. With the growth of scales, spherical (G-6m), block-shaped (C-6m and D-6m), needle-like (D-6m) and columnar (D-6m) crystals were generated and composed dense aggregations. At the same time, the crystalline size also increased with the corrosion process. Comparing the three types of scales, ductile iron had the most complex crystal structures and minimum porosity, which indicates that iron oxides had high degree of oxidation and could provide a more protective effect on the iron pipe.

Table 4 shows the elemental analysis results of the corrosion scales. In the table, iron (Fe) and oxygen (O) are the main components of all types of corrosion scales, with mass percentages of 74.09~87.00% (grey cast iron), 81.53~86.62% (carbon steel), and 88.64~90.22% (ductile iron). This

indicates that iron oxide is the main corrosion product, and ductile iron has the maximum proportion of iron oxides. In addition, there are small amounts of carbon (C) and silicon (Si), which mainly come from the metal matrix, since tap water contains almost none of these elements. Calcium (Ca) appeared in the scales and slightly increased in content with increased corrosion time. Thus, it can be speculated that Ca will deposit on the corrosion scales and promote the anti-corrosion effect of the corrosion scales.

Table 4. EDS analysis of the elemental composition of corrosion scale samples[a]

Sample	C	O	Si	Ca	Fe
G-1m	11.43	47.39	0.92	0.65	39.61
G-3m	24.43	52.57	0.8	0.68	21.52
G-6m	11.78	49.18	0.44	1.18	37.42
C-1m	16.72	55.69	1.24	0.51	25.84
C-3m	10.74	41.95	1.50	1.14	44.67
C-6m	11.77	50.18	1.62	0.96	35.47
D-1m	8.00	45.04	1.05	0.73	45.18
D-3m	9.20	46.72	0.82	1.03	42.23
D-6m	8.81	46.91	1.43	1.12	41.73

[a]All values are in atom% with an error of ±5%

The intensity of the XRD diffraction peak shows that iron oxide and hydroxyl oxidize iron are the predominant minerals in the scales. Goethite (α-FeOOH), lepidocrocite (γ-FeOOH), and magnetite (Fe_3O_4) are the main products of the grey cast iron scales; the scales of carbon steel are mainly composed of α-FeOOH, γ-FeOOH, and calcite ($CaCO_3$); α-FeOOH, γ-FeOOH, Fe_3O_4, $CaCO_3$, and siderite ($FeCO_3$) were also found in the first three months of scales of ductile iron. Thus, α-FeOOH and γ-FeOOH are the most basic corrosion products, which is consistent with the existing literature[21, 22]. Different from existing research results [12], green rusts (GRs) are not examined in the dry scale samples. GRs may transform into the more stable α-FeOOH and γ-FeOOH in the drying process of the samples.

The α-FeOOH content in all scale samples was high, while the intensity of γ-FeOOH showed an obvious fluctuation; it was very low in grey cast iron scales and increased with corrosion time in carbon steel and ductile scales. The reason may be that the crystal structure of α-FeOOH has lower free energy than γ-FeOOH, and in the long-term corrosion process, unstable γ-FeOOH can spontaneously and gradually transform into stable α-FeOOH. In addition, $CaCO_3$ only existed in the scales of carbon steel and ductile iron and was not detected in grey cast iron. Due to its poor electrical conductivity and strong adhesion, $CaCO_3$ can be combined with other iron oxidation products to significantly enhance the stability of the corrosion scale layer. Thus, with the deposition of $CaCO_3$, the corrosion rate of carbon steel and ductile iron is significantly lower than that of grey cast iron, which confirms that $CaCO_3$ is a highly effective component of the scales in terms of corrosion resistance. In contrast, the

intensity of the $CaCO_3$ peak in ductile iron was higher than that in carbon steel. One possible reason for this is that ductile iron generates more types of minerals with different sizes and structures, which is beneficial to the deposition of $CaCO_3$.

Previous result [13] found that the mass ratio of magnetite to goethite (M/G) can be used to evaluate the performance of cast iron pipe scales. But in this study, there was no magnetite being examined in the carbon steel scales, and the ratio of M/G is not suitable for evaluating the steel scales. Considering the constituent characteristics of all pipe scales, a more general criterion for evaluation of iron based pipe corrosion scale is proposed: high contents of α-FeOOH and CaCO3 are the symbol of the formation of an effective corrosion-control scale layer.

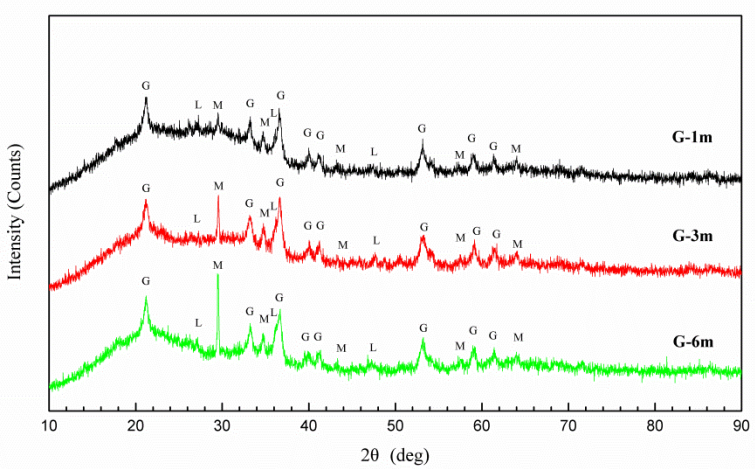

(a) Grey cast iron

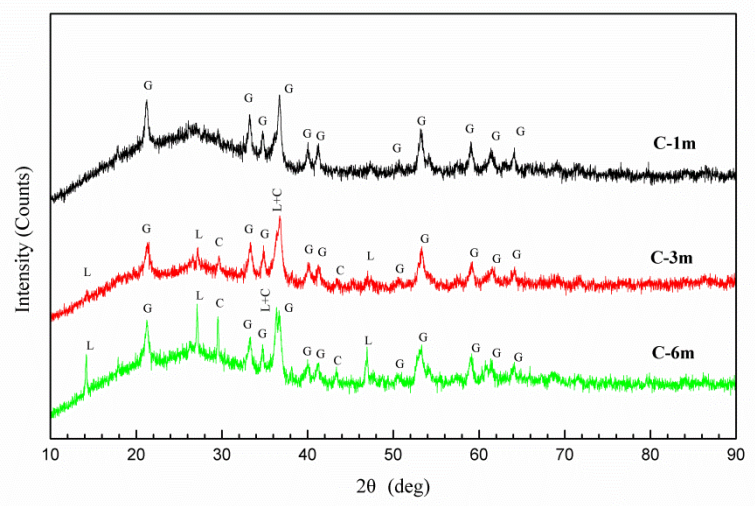

(b) Carbon steel

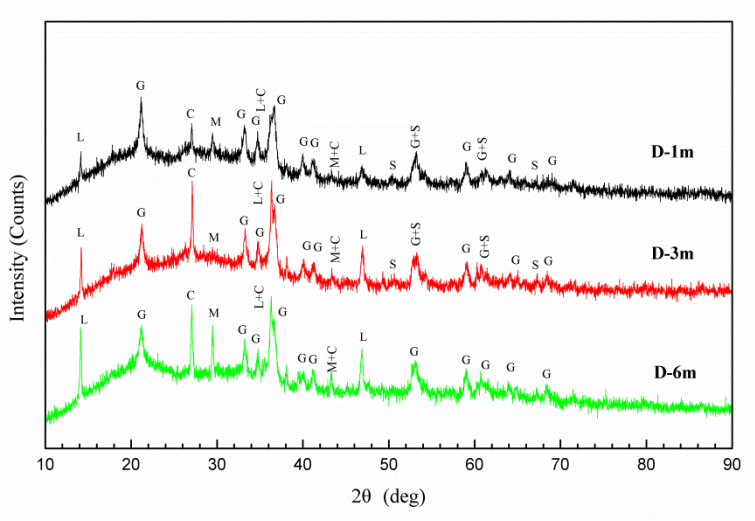

(c) Ductile iron

Figure 9. XRD patterns of the corrosion scales at different corrosion time of the 1st, 3rd and 6th month. G, L, M, C and S denote Goethite (α-FeOOH), lepidocrocite (γ-FeOOH), magnetite (Fe_3O_4), calcite ($CaCO_3$) and siderite ($FeCO_3$).

4. CONCLUSIONS

A 6-month circulating corrosion experiment was conducted through the SFCD and a specific EMC. In this study, test coupons were first immersed in the SFCD to generate a corrosion product layer similar to the actual inner-wall corrosion scales of WDS pipes. Then, one of the corroded coupons was directly fixed to the EMC as the working electrode for the electrochemical measurement, and the others were used for the corrosion rate measurement and scale morphology and physicochemical analyses. Thus, the weight-loss method and electrochemical measurement were integrated to study the corrosion behaviour and scale growth of iron pipes in WDSs.

With the increasing duration of the corrosion experiment in flowing drinking water, the coupon surface generated irregular corrosion scales. The scale characteristics varied with the material and corrosion environment and resulted in different corrosion behaviours. The coupon tests showed that grey cast iron had an obviously higher corrosion rate than carbon steel and ductile iron, which indicates that the corrosion products of the latter two have good corrosion inhibition effects. Considering the scale morphology, we can conclude that ductile iron has the lowest corrosion rate and most stable corrosion scales.

The EIS analysis confirmed that corrosion scales effectively controlled the electrochemical reaction, and the outer layer was more protective against pipe corrosion. However, for the ductile iron, both the outer and inner layers of scales are sufficiently dense to inhibit the corrosion process, which gives ductile iron a lower corrosion rate than grey cast iron and carbon steel.

The scale physicochemical analysis displayed the diversity of corrosion product composition and revealed the protect mechanism of the pipe scales: high contents of stable α-FeOOH and $CaCO_3$ deposition are beneficial to the formation of an effective corrosion-control scale layer.

ACKNOWLEDGEMENTS
We are grateful for the support provided by the National Natural Science Foundation of China (No. 51808158) and the Basal Scientific Research Funds of Central Public Welfare Scientific Institution (K-JBYWF-2018-CR05).

References

1. X. Li, Y. Wang and H. Zhao, *J. Harbin Inst. Technol.*, 33 (2001) 592.
2. L. S. Mcneill and M. Edwards, *J. Am. Water Works Assn.*, 93 (2001) 88.
3. X. Liu, Y. Tian, H. Guo, Y. Cheng, and L. Meng, *Corros. Sci. Prot. Technol.*, 27 (2015) 459.
4. S. Masters, H. Wang, A. Pruden and M. Edwards, *Water Res.*, 68 (2015) 140.
5. H. Wang, Master Dissertation of Zhejiang University. (2013) Zhejiang, China.
6. M. Sancy, Y. Gourbeyre, E. M. M. Sutter and B. Tribollet, *Corros. Sci.*, 52 (2010) 1222.
7. J. F. Rios, J. A. Calderón and R. P. Nogueira, *Corrosion*, 69 (2013) 875.
8. M. Fabbricino and G. V. Korshin, *Water Res.*, 62 (2014)136.
9. Y. Zou, J. Wang and Y. Y. Zheng, *Corros. Sci.*, 53 (2011) 208.
10. H. Guo, Y. Tian, H. Shen, Y. Liu and Y. Chen, *Int. J. Electrochem. Sci.*, 11 (2016) 6993.
11. Y. Tian, C. Liu, H. Guo, H. Zhang, X. Liu and Y. Chen, *Int. J. Electrochem. Sci.*, 13 (2018) 10023.
12. J. Świetlik, U. Raczyk-Stanisławiak, P. Piszor and J. Nawrocki, *Water Res.*, 46 (2012) 1.
13. F.Yang, B. Shi, J. Gu, D. Wang and M. Yang, *Water Res.*, 46 (2012) 5423.
14. X. Li, H. Wang, Y. Zhang, C. Hu and M. Yang, *Int. Biodeterior. Biodegrad.*, 96 (2014) 71.
15. X. Li, H. Wang, C. Hu, M. Yang, H. Hu and J. Niu, *Corros. Sci.*, 90 (2015) 331.
16. H. Wang, C. Hu, S. Zhang, L. Liu and X. Xing, *J. Environ. Sci.*, 73 (2018) 38.
17. J. Hu, H. Dong, W. Ling, J. Qu and Z. Qiang, *Water Res.*, 129 (2018) 428.
18. B. F. Trueman and G. A. Gagnon, *Environ. Sci. Technol.*, 50 (2016) 9053.
19. H. Sun, B. Shi, F.Yang and D. Wang, *Water Res.*, 114 (2017) 69.
20. G. Li, Y. Ding, H. Xu, J. Jin and B. Shi, *Chemosphere*, 197 (2018) 73.
21. P. Sarin, V. L. Snoeyink, J. Bebee, W. M. Kriven and J. A. Clement, *Water Res.*, 35 (2001) 2961.
22. T. L. Gerke, J. B. Maynard, M. R. Schock and D. L. Lytle, *Corros. Sci.*, 50 (2008) 2030.
23. M. Sfaira, A. Srhiri, H. Takenouti, M. Marie de Ficquelmont-Loïzos, A. Ben Bachir and M. Khalakhil, *J. Appl. Electrochem.*, 31 (2001) 537.
24. S. Dalbinc, G. Maurina, R. P. Nogueiraa, J. Persellob and N. Pommierc, *Surf. Coat. Technol.*, 194 (2005) 363.
25. L. Bousselmi, C. Fiaud, B. Tribollet and E. Triki, *Electrochim. Acta*, 44 (1999) 4357.
26. B. Yeum, Technical note 24 - pseudocapacitance associated with CPE, in: ZSimpWin Programme, EChem Software, 2002.
27. P. Sarin, V. Snoeyink, D. A. Lytle, and W. M. Kriven, *J. Environ. Eng.*, 130 (2004) 364.

© 2020 The Authors. Published by ESG (www.electrochemsci.org). This article is an open access article distributed under the terms and conditions of the Creative Commons Attribution license (http://creativecommons.org/licenses/by/4.0/).